

## Article

# Groundwater Hydrogeochemistry Impacted by Industrial Activities in Ain Sukhna Industrial Area, North-Western Part of the Gulf of Suez, Egypt

Hezam Al-Awah <sup>1</sup>, Mostafa Redwan <sup>2,\*</sup> and Shaymaa Rizk <sup>2</sup>

<sup>1</sup> Geology Program, Department of Chemistry and Earth Sciences, College of Arts and Sciences, Qatar University, Doha P.O. Box 2713, Qatar; hezam@qu.edu.qa

<sup>2</sup> Geology Department, Faculty of Science, Sohag University, Sohag 82524, Egypt

\* Correspondence: mostafa.redwan@science.sohag.edu.eg; Tel.: +20-934-605-602-2918

**Abstract:** Economic development and human life depend on groundwater resources in arid regions around the world. To define water quality in the Northwest Gulf of Suez, its elements, geogenic and anthropogenic sources, and suitability for various purposes, ten groundwater samples were collected and analyzed from wells tapping Quaternary and Tertiary aquifers. Average ion distribution was in the following order:  $\text{Na}^+ > \text{Mg}^{2+} > \text{Ca}^{2+} > \text{K}^+$  and  $\text{Cl}^- > \text{SO}_4^{2-} > \text{HCO}_3^-$ . Two water types with hydrochemical Ca-Mg-Cl-SO<sub>4</sub> facies accounted for 30% of samples due to reverse ion exchange, while Na-K-Cl-SO<sub>4</sub> accounted for 70% of samples due to evaporation. Cd (0–0.042 mg/L) and Pb (0–0.222 mg/L) from industrial applications in the study area exceeded the acceptable values in drinking water (>0.003 and 0.01 mg/L, respectively). Heavy metals and ionic value enrichment are due to weathering, precipitation/evaporation, ion exchange, and anthropogenic activities. Most ions in groundwater are higher than the acceptable limits prescribed for drinking water at all sites. Most groundwater in the investigated area is inappropriate for irrigation based on total salinity and MH index. High-salinity-tolerant plants and vegetables can be utilized according to the USSLS diagram. All groundwater samples have improper effects of incrustation and corrosion. Proper management actions are recommended to ameliorate the groundwater quality.

**Keywords:** groundwater; hydrogeochemistry; ion exchange; quality; element sources



check for updates

**Citation:** Al-Awah, H.; Redwan, M.; Rizk, S. Groundwater

Hydrogeochemistry Impacted by Industrial Activities in Ain Sukhna Industrial Area, North-Western Part of the Gulf of Suez, Egypt.

*Sustainability* **2023**, *15*, 12787.

<https://doi.org/10.3390/su151712787>

Academic Editors: Rayco

Guedes-Alonso, Sarah

Montesdeoca-Esponda and José

Alberto Herrera-Melián

Received: 25 July 2023

Revised: 8 August 2023

Accepted: 12 August 2023

Published: 24 August 2023



**Copyright:** © 2023 by the authors. Licensee MDPI, Basel, Switzerland.

This article is an open access article distributed under the terms and conditions of the Creative Commons Attribution (CC BY) license (<https://creativecommons.org/licenses/by/4.0/>).

## 1. Introduction

High-risk industries cause severe health effects for both workers and the nearby environment. Natural and anthropogenic contaminants in desert provinces govern water quality, and are definitive factors for sustainable development. Natural geogenic factors such as aquifer lithology, water–sediment interaction, precipitation, and groundwater flow are mostly affected by climatic variations, while anthropogenic factors are persistent polluting point sources in urban areas through point and non-point pollution sources such as residential wastewater, urbanization, agriculture, industrial effluent, sewage discharge, and/or atmospheric inputs [1–4]. Numerous soluble chemical components in diverse contents originate in water, where they are controlled by the interaction time of water-bearing sediments and biochemical anthropogenic factors [5]. Thus, recognizing the contrasting processes that impact groundwater quality is the key to attaining quality control and ensuring its amelioration plan.

Extensive projects have been established in the northwest Suez Gulf region by the Egyptian government for future economic development in the region. Accordingly, this area is a crucial investment zone and a notable source of Egyptian national income. Different investment projects include oil refineries, fertilizer and chemical industries, power stations, cement factories, and the establishment of enormous trading harbours close to the industrial zone. Furthermore, 450 freshly matured projects are intended in this zone,

such as steel manufacture, power plants, oil factories, ceramics, cements, and fiberglass [6]. The ecosystem in the investigated region is greatly impacted by such industrialization activities. The Suez Gulf and Suez Bay in the Red Sea are already greatly polluted by contaminants [7–9].

Concentrations of heavy metals such as lead and cadmium in Red Sea sediments have become elevated due to environmental pollution by five- and three times, respectively, during the 50 years from 1934 to 1984 [10]. These increases may be ascribed to oil pollution. Heavy metals (Cd, Pb, Cu, and Zn) due to industrial oil refinery effluents have been identified in fish gathered from the Suez Gulf [11]. Hamed and Said [12] indicated that the high eutrophic region (high productivity) in the Suez Bay area causes water quality deterioration as a result of acidic sewage and industrial and oil refinery effluents that are expanding along the western coast of the bay. Metals such as Cd, Co, Pb, and Ni have been found to exhibit greater mean values (0.53–0.75, 1.64–2.37, 1.36–1.43, and 2.06–4.66  $\mu\text{g/g}$ , respectively) in a few Red Sea marine organisms [13]. Rushdi et al. [14] stated that Suez Gulf coast sediments hold several different anthropogenic organic materials from petroleum activities. Abdel-Hamid et al. [15] recognized high levels of trace metals such as Pb, Co, Cd, Ni, and Fe in the north Red Sea in water and sediments (0.8, 0.52, 0.43, 5.80, and 28.35  $\mu\text{g/L}$  and 12.64, 13.29, 4.30, 18.0, and 1285.0  $\mu\text{g/g}$ , respectively). Shreadah et al. [16] recognized organometallic compounds from industrial discharge that have different toxicological behaviors in coastal sediments of the Suez Gulf. They concluded that industrial effluent is the chief pollution source in the Suez Gulf. Snousy et al. [17] recognized various polycyclic aromatic hydrocarbon (PAH) concentrations varying from 10.36 to 107.23  $\text{mg/kg}$  in sediments gathered from an industrial location adjacent to Suez Bay. Wind action and/or flash flooding, which commonly occur in the investigated region, disperse industrial waste, leading to pollution of groundwater aquifers.

As a result of a lack of knowledge regarding the characterization of groundwater aquifers in this area and many other areas around Egypt, this study was executed to: (1) evaluate the hydrogeochemical characteristics of groundwater, (2) identify the geogenic and anthropogenic sources of heavy element origins and variability, (3) evaluate water suitability for drinking, irrigation, and industrial use, and (4) study groundwater vulnerability with respect to the human population in the study area.

### 1.1. Study Area

Gable Akheider is situated in the Ain Sukhna industrial zone on the western side of the Gulf of Suez, Egypt (Figure 1). The study area expresses a portion of Tertiary plateau of the Northern Eastern Desert of Egypt. The region is enclosed by latitudes  $29^{\circ}44'$  and  $29^{\circ}36'$  N and longitudes  $31^{\circ}15'$  and  $32^{\circ}23'$  E, comprising an area of about 400  $\text{km}^2$ . The Suez Gulf is located in the eastern part of the study area. This side gently increases until it integrates into the Tertiary plateau of the Eastern Desert's northern part [18].

### 1.2. Geologic Setting

The exposed sequence is composed of pre- and syn-rift strata varying from Middle Eocene to Quaternary (Figure 1). The pre-rift sediments exist as tilted fault blocks aligned with the Gulf of Suez. These sediments start from bottom with carbonates of Middle Eocene Sannor Formation lying below mixed siliciclastic and carbonates of Upper Eocene Maadi Formation. The syn-rift sediments start with the red siliciclastic beds of the Late Oligocene Gabal El-Ahmar Formation. The red beds are overlain by the fossiliferous sandstone, marls, and clays of the Middle Miocene Hommath Formation. This is followed by massive bedded shale, siltstone, and calcareous sandstones of the Upper Miocene Hagul Formation [19,20]. Plio-Quaternary sediments consist of gravels, sands, and evaporites. The area is cut by a series of structurally controlled fault blocks, the majority of which attain a NW-SE direction, thereby generating topographic highs and lows [21]. The topographic highs are represented by the hard Middle Eocene Sannor Formation, while the lows are occupied by the soft Oligocene to recent ages. Gabal Akheider corresponds to one of these horst blocks (Figure 1).

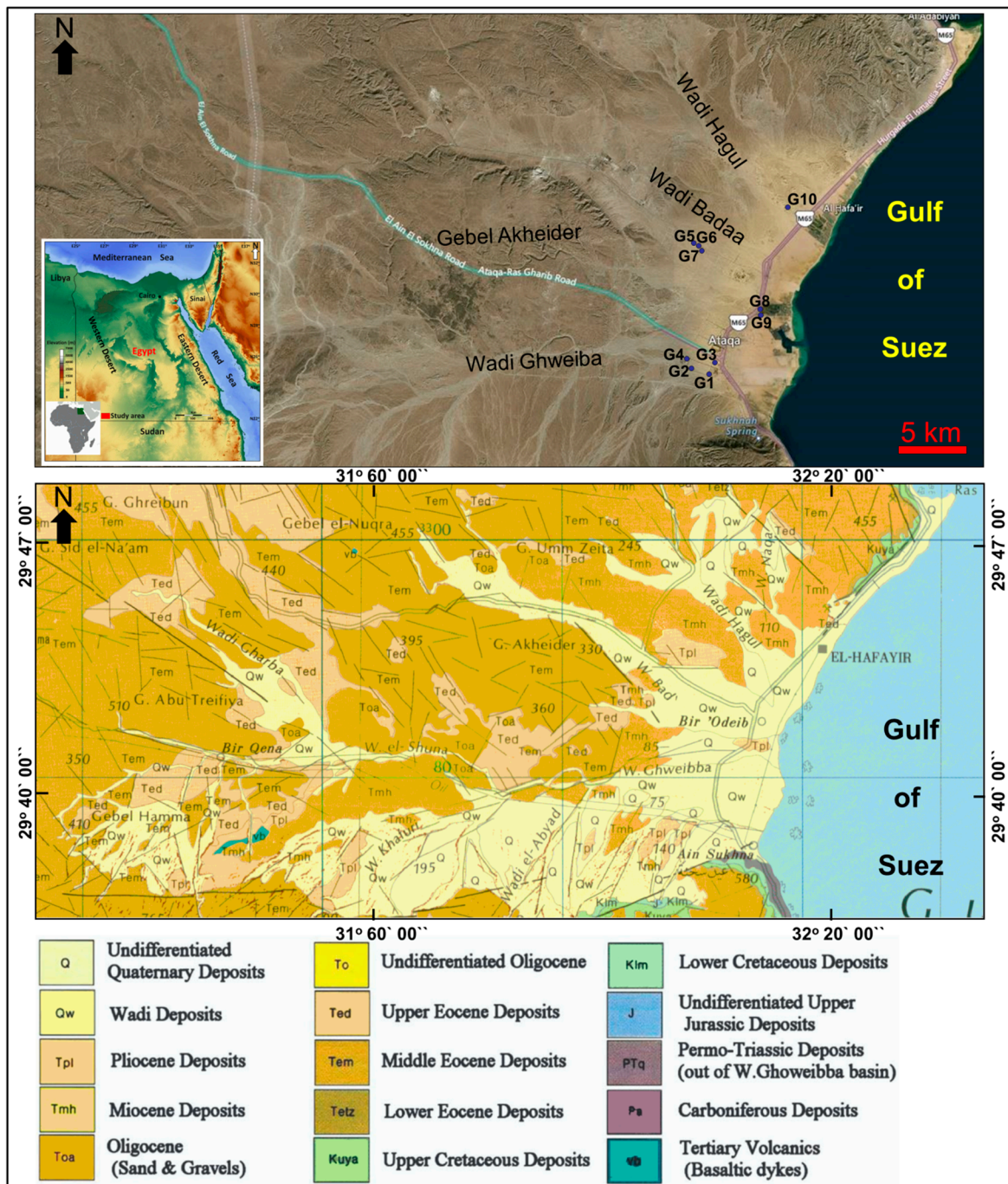


Figure 1. Location Google Earth and geologic maps of the study area and its surroundings (modified after [18]). Groundwater sampling sites from G1 to G10.

### 1.3. Climate

The Ain Sukhna zone is marked by an arid climate. The mean temperature is up to 9 °C in January and attains 36 °C in July. The mean relative humidity varies from 45% to 60%. The zone receives moderate quantities of rainfall (~60–75 mm/year), chiefly in autumn and winter [22,23].

## 2. Materials and Methods

### 2.1. Sampling and Field Methods

Ten representative groundwater samples were gathered from wells in the investigated area during November 2022. The sampling locations were specified based on populated in-

dustrial zones. The coordinates of sampling locations were indicated by Global Positioning System (Garmin 10). The wells were tapped from the Tertiary aquifers (Figure 2). Clear water pumping for 10 min was carried out to address the sampling of stagnant annulus water in the pump systems. The groundwater samples were kept in polyethylene bottles at 4 °C. Major ions and heavy metals were analyzed with appropriate QA/QC utilizing approved protocols [24].

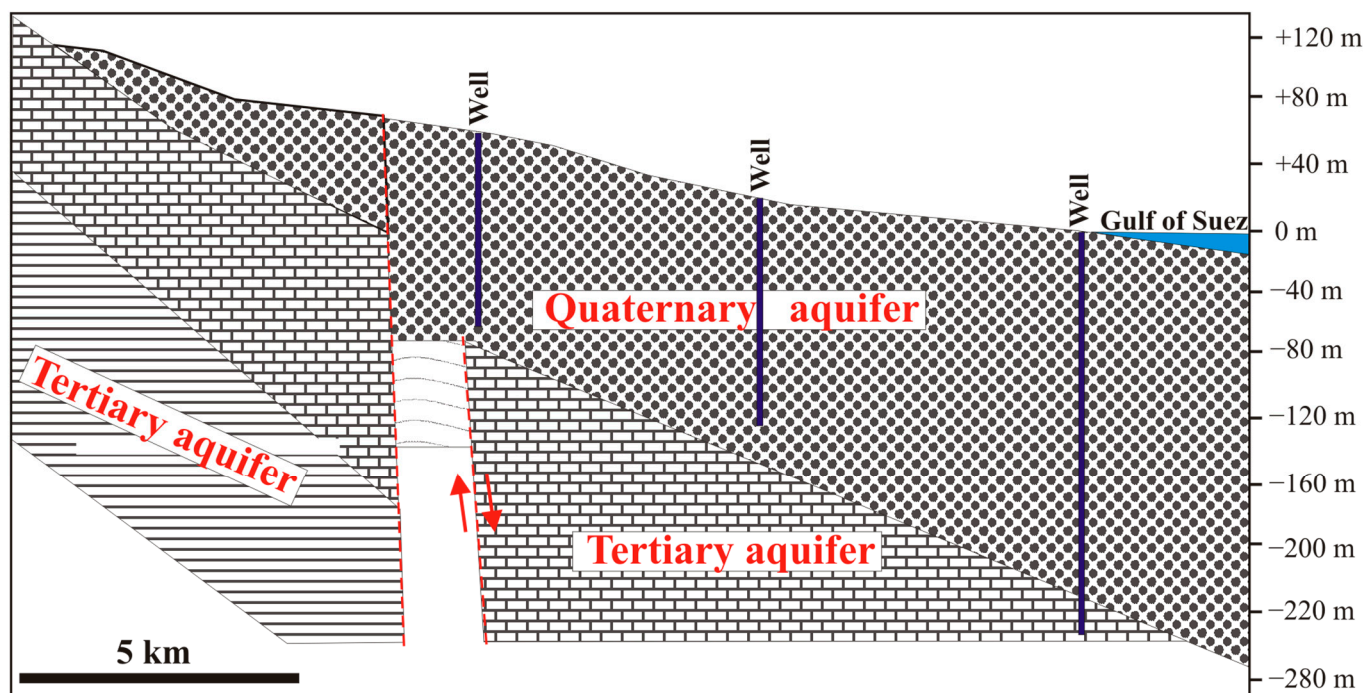


**Figure 2.** Schematic hydrogeological cross-section along the study area (modified after [25]). Arrows indicate the fault movement.

## 2.2. Geochemical Analyses

The groundwaters were divided into unacidified samples and used to measure pH, EC, TDS,  $\text{Cl}^-$ ,  $\text{SO}_4^{2-}$ ,  $\text{HCO}_3^-$ , and  $\text{NO}_3^-$ . Electrical conductivity (EC), total dissolved solids (TDS, ADWA Instruments, Inc., Szeged, Hungary), and pH quantifications in the field were performed by digital meters (Jenway Ltd. 4510, Essex, UK). The pH was calibrated at three points using (4.01, 7.00, and 10.01) buffer groups. Conductivity was calibrated with an automatic calibration at 84  $\mu\text{S}$  with a conductivity calibration standard. Double distilled deionized water was utilized for rinsing the glassware after cleaning with 2%  $\text{HNO}_3$  to forbid any interference in the result. The titration method was utilized for the quantification of  $\text{HCO}_3^-$  and  $\text{Cl}^-$ . The colorimetric and turbidimetric methods were used for  $\text{SO}_4^{2-}$  and  $\text{NO}_3^-$  determination. The acidified samples using 6 N nitric acid were used to measure cations ( $\text{Ca}^{2+}$ ,  $\text{Mg}^{2+}$ ,  $\text{Na}^+$ ,  $\text{K}^+$ ) and heavy metals (Cd, Cu, Fe, and Pb). The chemical analyses of major cations and heavy metals were performed using an Atomic Absorption Spectrometer (AAAnalyst 400, PerkinElmer, Inc., Shelton, CT, USA). Analytical grade reagents (Merck, Germany) were utilized to ensure reliability. To obtain the highest measurement accuracy and quality control, analysis of groundwater was executed in duplicate and proper standards and blanks were used with the greatest purity grade chemicals. The AquaChem software 2014 version (Waterloo Hydrogeologic, Inc., Waterloo, ON, Canada) was utilized for plotting the relative concentrations of ions.

## 2.3. Ion Exchange Process

To identify the purpose of ion exchange in the aquifers, the chloro-alkaline indices (CAI-1 and CAI-2) [26] were calculated (Equations (1) and (2)). A negative index of CAI

(reverse ion exchange) demonstrates that  $\text{Ca}^{2+}$  and  $\text{Mg}^{2+}$  in groundwater replace  $\text{Na}^+$  and  $\text{K}^+$  in aquifer material [27]. A positive CAI index (base ion exchange process) demonstrates the release of  $\text{Ca}^{2+}$  and  $\text{Mg}^{2+}$  and adsorption of  $\text{Na}^+$  and  $\text{K}^+$  ions in the aquifer.

$$\text{CAI-1} = \frac{\text{Cl}^- - (\text{Na}^+ + \text{K}^+)}{\text{Cl}^-} \quad (1)$$

$$\text{CAI-2} = \frac{\text{Cl}^- - (\text{Na}^+ + \text{K}^+)}{\text{HCO}_3^- + \text{SO}_4^{2-} + \text{CO}_3^{2-} + \text{NO}_3^-} \quad (2)$$

#### 2.4. Suitability for Irrigation Purpose

Residual sodium carbonate (RSC), shown in Equation (3) [28], is among the key criteria used to quantify groundwater's suitability for agriculture.  $\text{Ca}^{2+}$  and  $\text{Mg}^{2+}$  precipitate when  $\text{HCO}_3^-$  and  $\text{CO}_3^{2-}$  exceed  $\text{Ca}^{2+}$  and  $\text{Mg}^{2+}$ . An elevated RSC value denotes that ions merge with  $\text{Ca}^{2+}$  and  $\text{Mg}^{2+}$  precipitate. Thus, more sodium adsorption in soil causes sodium hazard. Elevated carbonate values can unite with  $\text{Na}^+$  to create  $\text{NaHCO}_3$ , which affects soil structure. RSC (Equation (3), in meq/L) is concerned with the carbonate content of water [29].

$$\text{RSC} = (\text{CO}_3^{2-} + \text{HCO}_3^-) - (\text{Ca}^{2+} + \text{Mg}^{2+}) \quad (3)$$

Magnesium Hazard (MH) was evaluated using the Szabolcs and Darab equation [30], where the concentration of each cation was expressed in meq/L:

$$\text{MH} = \left( \frac{\text{Mg}^{2+}}{\text{Ca}^{2+} + \text{Mg}^{2+}} \right) \times 100 \quad (4)$$

The USSLS [31] suggests a sodium adsorption ratio (SAR, in meq/L) due to its exact connection to soil adsorption (Equation (5), meq/L).

$$\text{SAR} = \frac{\text{Na}^+}{\sqrt{\frac{\text{Ca}^{2+} + \text{Mg}^{2+}}{2}}} \quad (5)$$

The USSLS plots the conductivity (in micro-mhos/cm at 25 °C) against SAR. It is separated into sixteen regions depending on sodium hazards. A high SAR value reflects a cation exchange saturated with  $\text{Na}^+$ , as water has an elevated  $\text{Na}^+$  value. It additionally indicates a low concentration of  $\text{Ca}^{2+}$ , which destroys the soil structure by dispersion of clay particles. The salinity hazard (C) can be split into four sub-zones: low salinity (C1, <250  $\mu\text{S}/\text{cm}$ ), medium salinity (C2, 250 to 750  $\mu\text{S}/\text{cm}$ ), high salinity (C3, 750 to 2250  $\mu\text{S}/\text{cm}$ ), and very high salinity (C4, >2250  $\mu\text{S}/\text{cm}$ ), which have good, moderate, poor, and very poor water classes, respectively. Equivalently, sodium hazards (S) are split into four sub-zones: low sodium (S1, <10), medium sodium (S2, 10 to 18), high sodium (S3, 18 to 26), and very high sodium (S4, >26), which have good, moderate, poor, and very poor water classes, respectively.

#### 2.5. Suitability for Industrial Purposes

The corrosivity ratio (CR) quantifies groundwater's appropriateness for industrial purposes. This ratio displays the corrosion grade of metal pipes. Equation (6) denotes the CR ratio of alkaline earths to saline salts (in mg/L). A  $\text{CR} > 1$  reflects water's unsuitability for industrial use [32].

$$\text{CR} = \left( \frac{\text{Cl}^-}{35.5} + \frac{\text{SO}_4^{2-}}{48} \right) / \left( \frac{\text{CO}_3^{2-} + \text{HCO}_3^-}{50} \right) \quad (6)$$

### 3. Results and Discussions

#### 3.1. Hydrogeological Setting

The groundwater in this area was examined by analyses of the hydrogeological data obtained from ten drilled wells (Table 1) as well as by the assessment of accessible information linked to geology and hydrogeology. The groundwater aquifers exist in contrasting states, indicating significant structural, lithological, and elevation changes. Groundwater is the principal water source in the arid zone, and is utilized for agricultural and industrial purposes. Numerous wells have been drilled by companies in Ain Sukhna to draw out water for industrial applications.

**Table 1.** Groundwater parameters in the study area.

Ser.No	Location	Lat-N	Long-E	Depth-m	Aquifer
G1	Ghweiba basin	29.63	32.30	70	Quaternary aquifer
G2	Ghweiba basin	29.63	32.29	129	Quaternary aquifer
G3	Ghweiba basin	29.63	32.30	150	Quaternary aquifer
G4	Ghweiba basin	29.63	32.29	120	Quaternary aquifer
G5	Badaa basin	29.72	32.27	144	Quaternary aquifer
G6	Badaa basin	29.72	32.28	144	Quaternary aquifer
G7	Badaa basin	29.72	32.28	146	Quaternary aquifer
G8	Badaa basin	29.67	32.34	128	Tertiary aquifer
G9	Badaa basin	29.67	32.34	117	Quaternary aquifer
G10	Hagul	29.73	32.37	75	Quaternary aquifer

Depending on the geology and stratigraphy of the study region, the water-bearing formations are grouped into Tertiary (Miocene carbonate and Pliocene deposits) and Quaternary alluvial (sand, silt, and gravel) aquifers (Figure 2). The groundwater in the desert zone is indicated by a sand, silt, and gravel succession related to Quaternary deposits. The Quaternary aquifer overlies the carbonate group of sediments (Eocene). The Quaternary aquifer is the chief aquifer in the area. The penetrated thickness of this aquifer in the mouth of Wadi Ghweiba attains about 400 m, decreasing towards the north and northeast. The groundwater exists in a free water table state. The depth ranges between 70 and 150 m from the ground surface. Variations in depth are due to the effects of faults on the relief of this area [33]. An isotopic study has shown that runoff and upward leakage/downward infiltration from deep aquifers are the main recharge sources [34]. The depth to water increases gradually from the SE towards the NW. The Tertiary aquifer is located in Wadi Bada. It is mostly composed of limestone, clay, sand, and gravel with dolomite. The Tertiary aquifer is chiefly recharged from the Quaternary aquifer, along with direct infiltration as well as seepage from deep aquifers. The discharge occurs through fissures to other aquifers or by pumping. The groundwater in this aquifer is under confined conditions.

Wadi Hagul basin is marked by a low seepage rate; a major flooding period of  $3.24 \times 10^6 \text{ m}^3$  happened in 1990, with a runoff rate of  $2.26 \times 10^6 \text{ m}^3/\text{h}$  and a seepage rate of  $0.71 \times 10^6 \text{ m}^3/\text{h}$ . The seepage–runoff relationship in Wadi Badaa basin indicates that this wadi is modest in its accumulation of floodwater, though a large flood rate of  $5.06 \times 10^6 \text{ m}^3/\text{h}$  occurred in 1990 with a seepage rate of  $2.93 \times 10^6 \text{ m}^3/\text{h}$ . Wadi Ghweiba basin had an elevated runoff rate of  $22.8 \times 10^6 \text{ m}^3/\text{h}$  in 1990, with a seepage rate of  $9.70 \times 10^6 \text{ m}^3/\text{h}$  [35].

#### 3.2. Hydrogeochemistry

##### 3.2.1. Groundwater Geochemistry

Various items govern the groundwater geochemistry in the aquifers. These factors include rock type, residence time, initial groundwater composition, and water flow path [36]. The chemical composition of the groundwater in the investigated area is exhibited in Table 2. The pH values of groundwater ranged from 6.91 to 8.02 in the Quaternary aquifer and 7.12

in the Tertiary aquifer, depicting neutral to lightly alkaline water in the investigated area. All groundwater samples are in the safe limit of pH (6.5 to 8.5).

**Table 2.** Chemical (in mg/L) and physical properties of groundwater. EC: electrical conductivity in  $\mu\text{S}/\text{cm}$ .

Ser.No	pH	EC	TDS	K <sup>+</sup>	Na <sup>+</sup>	Mg <sup>2+</sup>	Ca <sup>2+</sup>	Cl <sup>-</sup>	SO <sub>4</sub> <sup>2-</sup>	HCO <sub>3</sub> <sup>-</sup>	NO <sub>3</sub> <sup>-</sup>	Cd	Cu	Pb	Fe	TH	CR
G1	7.23	5320	3558	34	826	171	211	1384	645	265	16.2	0.014	0.0025	0.022	0	1229	9.89
G2	7.06	4274	2589	27	470	188	205	1190	405	82	0	0	0.024	0.082	0	1283	25.58
G3	7.32	5570	4081	24	934	172	254	1699	595	381	2	0.042	0	0.112	0	1340	7.91
G4	6.91	7070	3420	30	280	425	351	1779	395	137	2.1	0	0.004	0.222	0.006	2620	21.29
G5	6.96	4569	2763	13	631	89	230	1254	395	129	0.92	0.031	0.0024	0.162	0.004	940	16.88
G6	7.03	3750	3174	6.5	782	88	225	1174	395	482	0.84	0.006	0.0034	0.182	0	923	4.28
G7	7.68	1430	2543	11	167	232	337	877	405	492	1.2	0.024	0	0.192	0.0021	1794	3.37
G8	7.12	11,340	6841	8.3	1504	332	528	3327	995	127	2.8	0.021	0	0.022	0.0401	2681	45.06
G9	7.34	7670	5123	10.3	1184	255	368	2427	745	112	6	0.005	0	0.122	0.014	1966	37.45
G10	8.02	7620	2450	12	514	105	191	1026	220	365	0	0	0	0.132	0.021	908	4.59

The slight increase of pH in the groundwater is due to rock weathering, leaching from industry (limestone, steel, cement plants), and agricultural and municipal waste. These activities cause HCO<sub>3</sub><sup>-</sup> ion influx in the aquifer by downward infiltration of rainwater [32,37,38]. The salinity ranges from 2543 to 5123 mg/L in the Quaternary aquifer and 6841 mg/L in the Tertiary aquifer (Table 2). Lesser concentrations are recognized along the northwestern part of the investigated area, which manifest an absence of marine facies (topographic highs) and homogeneity of aquifer materials. Elevated concentrations are recognized in the eastern part near the coast of the Gulf of Suez (topographic lows), manifesting in leaching of marine gypsiferous shale and clay [38] prevailing in the downstream direction in the investigated area. High TDS values in the investigated area indicate the long residence time of groundwater with high weathered sediments or seawater invasion [32]. The nonlinearity observed in EC with TDS may be in regard to the ion–ion and ion–solvent interactions becoming more substantial. The sulfates exhibit comparable trends to the salinity, with elevated values in the east near the coast (topographic lows) (Table 2).

The average dispersal of major ions in the groundwater follows the order Na<sup>+</sup> > Mg<sup>2+</sup> > Ca<sup>2+</sup> > K<sup>+</sup> and Cl<sup>-</sup> > SO<sub>4</sub><sup>2-</sup> > HCO<sub>3</sub><sup>-</sup>. The Na<sup>+</sup> value shows a great disparity from 167 to 1184 mg/L in the Quaternary aquifer and 1504 mg/L in the Tertiary aquifer. Most groundwater has Na<sup>+</sup> values higher than the allowable value of drinking water (200 mg/L) [39]. Ion exchange and leaching of sodium salts is the chief Na<sup>+</sup> source [40]. The Ca<sup>2+</sup> ion value varies between 191–368 mg/L in the Quaternary aquifer and 528 mg/L in the Tertiary aquifer. According to drinking water standards [39], all groundwater surpasses the allowable value of 75 mg/L [39]. Carbonate and/or silicate dissolution are the major sources of Ca<sup>2+</sup> enrichment in groundwater. The Mg<sup>2+</sup> concentration ranges from 88 to 425 mg/L in the Quaternary aquifer and 332 mg/L in the Tertiary aquifer. Mg<sup>2+</sup> enrichment in groundwater is due to dissolution of dolomite and/or silicate minerals. All concentrations exceed the allowable drinking limit of 50 mg/L. The K<sup>+</sup> value varies from 6.5 to 34 mg/L in the Quaternary aquifer and 8.3 mg/L in the Tertiary aquifer.

Sulfate varies between 220 and 745 mg/L in the Quaternary aquifer and 995 mg/L in the Tertiary aquifer. The SO<sub>4</sub><sup>2-</sup> value is higher than the allowable value of 200 mg/L [39]. The chloride distribution varies from 877 mg/L to 2427 mg/L in the Quaternary aquifer and 3327 mg/L in the Tertiary aquifer near the coast (Table 2). Cl<sup>-</sup> values are higher than the allowable drinking limit of 200 mg/L [39]. Elevated Cl<sup>-</sup> amounts manifest a dissolution of Cl-bearing deposits such as halite, gypsiferous shale, and clays [38,41] prevailing in the coastal aquifer materials. Bicarbonate values range between 82 mg/L and 492 mg/L in the Quaternary aquifer and 127 mg/L in the Tertiary aquifer near the coast (Table 2). Higher carbonate values were recorded in the western part of the investigated area near Gebel Akheider. HCO<sub>3</sub><sup>-</sup> values are reversibly comparable to other ion values in most samples in the investigated area (except samples G6 and G7), which can be assigned to an ion exchange

reaction [41,42]. Nitrate values in the investigated area vary between 0 and 16.2 mg/L (Table 2). A higher value was recognized in sample G1 in the southeastern part (Figure 1).  $\text{NO}_3^-$  does not have a lithological source. In a natural environment,  $\text{NO}_3^-$  values do not exceed 10 mg/L in water [43]. Different factors affect  $\text{NO}_3^-$  pollution in groundwater, such as agricultural and land use activities (villages, poultry factories, etc.) [44–47]. The sources of  $\text{Cl}^-$ ,  $\text{SO}_4^{2-}$ ,  $\text{NO}_3^-$ , and  $\text{Na}^+$  ions are chiefly agriculture, industry, animal waste, and municipal sewage [44,48]. The elevated total hardness quantity in water causes an unpleasant taste and decreases the capability of soap to generate lather. According to the hardness classification ( $\text{TH} = 2.5 \text{ Ca} + 4.1 \text{ Mg}$ ) of Kilemntov [49], three samples fall into the moderate water type (G5, G6, G10) (250–1000 mg/L) and the rest fall in the hard water type (>1000 mg/L).

The cadmium (Cd) value in the groundwater ranges from 0 mg/L to 0.042 mg/L in the Quaternary aquifer and 0.021 mg/L in the Tertiary aquifer. The maximum Cd value in drinking water is 0.003 mg/L [39]. Source may include from smelting copper ores, pigments, paint, ceramics, plastics, fertilizers, and sewage waste [50]. Cd can cause giddiness, respiratory problems, and a decrease in consciousness, while elevated amounts cause anaemia, anosmia, renal problems, hypertension, and cardiovascular diseases [51]. The lead (Pb) value in groundwater ranges from 0 mg/L to 0.222 mg/L in the Quaternary aquifer and 0.022 mg/L in the Tertiary aquifer. All samples exceed the acceptable Pb values in drinking water (>0.01 mg/L) [39]. Pb may result from smelting, motor vehicle exhaust fumes, and lead pipework corrosion [52]. Lead exposure results in tiredness, anaemia, irritability, and impairment of intellectual functions [53]. Copper showed enrichment at several wells, which may be related to industrial applications such as paint, plumbing pipes, and storage batteries [50]. Domestic and industrial wastewater discharged in the study area could increase the concentrations of Cd, Cu, and Pb metal. The ionic and heavy metal values rely on rock weathering, precipitation, leaching, and anthropogenic activities.

### 3.2.2. Ion Sequence and Ratio

Generally, elevated ion values in groundwater happen due to weathering of silicate rocks and anthropogenic activities. Evaporation increases the chemical budget of groundwater. The chief ion sequence of crucial elements in this area (Figure 3, Table 3) based on Schoeller's semi logarithmic charts [54], achieves four sequences as follows:

**Table 3.** Hydrochemical ion ratios of groundwater in the investigated area.

Ser.No	$r\text{Na}^+/\text{rCl}^-$	$r\text{SO}_4^{2-}/\text{rCl}^-$	$r\text{Ca}^{2+}/\text{rMg}^{2+}$	$r\text{Ca}^{2+}/\text{rNa}^+$	$r\text{Ca}^{2+} + r\text{Mg}^{2+}/\text{rHCO}_3^-$	RSC	MH
G1	0.92	0.34	0.75	0.29	5.66	−20.25	57.2
G2	0.61	0.25	0.66	0.50	19.11	−24.35	60.2
G3	0.85	0.26	0.90	0.31	4.29	−20.57	52.7
G4	0.24	0.16	0.50	1.44	23.36	−50.22	66.6
G5	0.78	0.23	1.57	0.42	8.89	−16.68	38.9
G6	1.03	0.25	1.55	0.33	2.34	−10.56	39.2
G7	0.29	0.34	0.88	2.31	4.45	−27.83	53.2
G8	0.70	0.22	0.97	0.40	25.77	−51.57	50.9
G9	0.75	0.23	0.88	0.36	21.43	−37.50	53.3
G10	0.77	0.16	1.10	0.43	3.04	−12.18	47.5

$\text{Na}^+ > \text{Mg}^{2+} > \text{Ca}^{2+}/\text{Cl}^- > \text{SO}_4^{2-} > \text{HCO}_3^-$  (about 50% of the analyzed water samples, G1, G2, G3, G8 and G9).

$\text{Na}^+ > \text{Ca}^{2+} > \text{Mg}^{2+}/\text{Cl}^- > \text{SO}_4^{2-} > \text{HCO}_3^-$  (about 20% of the analyzed water samples, G5 and G6).

$\text{Mg}^{2+} > \text{Ca}^{2+} > \text{Na}^+/\text{Cl}^- > \text{SO}_4^{2-} > \text{HCO}_3^-$  (about 20% of the analyzed water samples, G4 and G7).

$\text{Na}^+ > \text{Ca}^{2+} > \text{Mg}^{2+} / \text{Cl}^- > \text{HCO}_3^- > \text{SO}_4^{2-}$  (about 10% of the analyzed water samples, G10).

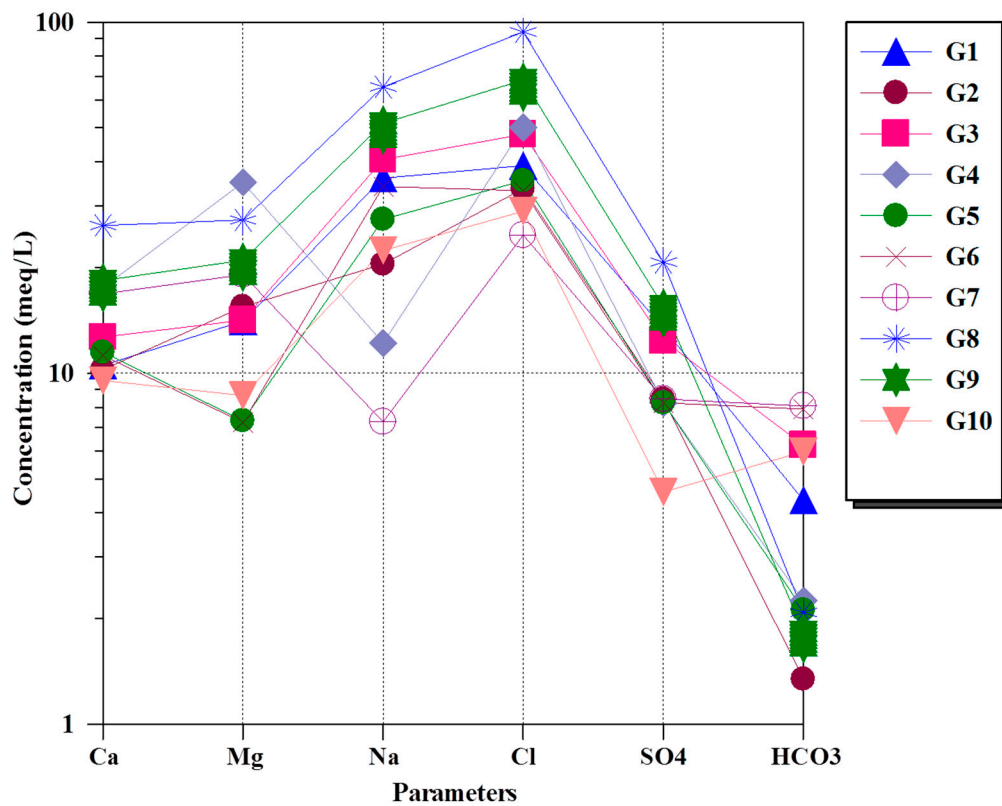


**Figure 3.** Schoeller diagram of the major ions in groundwater samples in the study area.

Sodium chloride, sodium sulfate, and magnesium chloride are the main water types. The prevalence of NaCl may be related to evaporites and dissolution of marine salts in the Quaternary aquifer [38,41], whereas  $\text{Na}_2\text{SO}_4$  indicates the dissolution of  $\text{SO}_4^-$  minerals and drained meteoric water [55] in the study area.

Ionic ratios in the investigated area have been utilized to assess the salinity and origin of groundwater [38]. The ionic associations utilized in this investigation involve  $r\text{Ca}^{2+}/r\text{Mg}^{2+}$ ,  $r\text{SO}_4^{2-}/r\text{Cl}^-$ , and  $r\text{Na}^+/r\text{Cl}^-$ . The  $r\text{Ca}^{2+}/r\text{Mg}^{2+}$  ratio ranges from 0.5 to 1.57 in the Quaternary aquifer and 0.97 in the Tertiary aquifer. The elevated ratio (samples G5 and G6) exhibits hydrolysis of Ca-bearing silicate minerals in basement rocks [56]. The  $r\text{SO}_4^{2-}/r\text{Cl}^-$  ratio varies between 0.16 and 0.34 in the Quaternary aquifer and 0.22 in the Tertiary aquifer. The elevated  $\text{SO}_4^{2-}$  in groundwater is related to local terrestrial sulfate rock dissolution [57]. The  $r\text{Na}^+/r\text{Cl}^-$  ratio of around one molar ratio indicates that halite dissolution is the chief  $\text{Na}^+$  source in the groundwater [57]. Higher  $r\text{Na}^+/r\text{Cl}^-$  ratio than 1 are explained as  $\text{Na}^+$  being delivered from silicate dissolution [58].  $r\text{Na}^+/r\text{Cl}^-$  ratios lower than one reflect that sodium is lost through reverse ion exchange [59]. The  $r\text{Na}^+/r\text{Cl}^-$  value in the investigated area varies from 0.24 to 1.03 in the Quaternary aquifer and 0.70 in the Tertiary aquifer, indicating halite dissolution and reverse ion exchange reactions.

### 3.2.3. Interrelations of Chemical Parameters

Equiline plots (Figure 4) for different the ions exhibit ion characteristics and their affinities. The plot of  $\text{Na}^+ + \text{K}^+$  vs.  $\text{Cl}^-$  (Figure 4a) shows that bulk values fall above and on the equiline, denoting that alkali ions are equal with  $\text{Cl}^-$  ions. Halite dissolution discharges equivalent  $\text{Na}^+$  and  $\text{Cl}^-$  ions in water. Figure 4a diverges from the 1:1 plot as a result of anthropogenic factors in the groundwater. The  $\text{Cl}^-$  in the groundwater is primary due to the dissolution of saline materials, sewage, and agricultural and industrial effluents

(anthropogenic sources). The values of  $\text{Na}^+$  obtained from silicate weathering are cloaked by anthropogenic inputs (i.e., domestic and industrial waste).

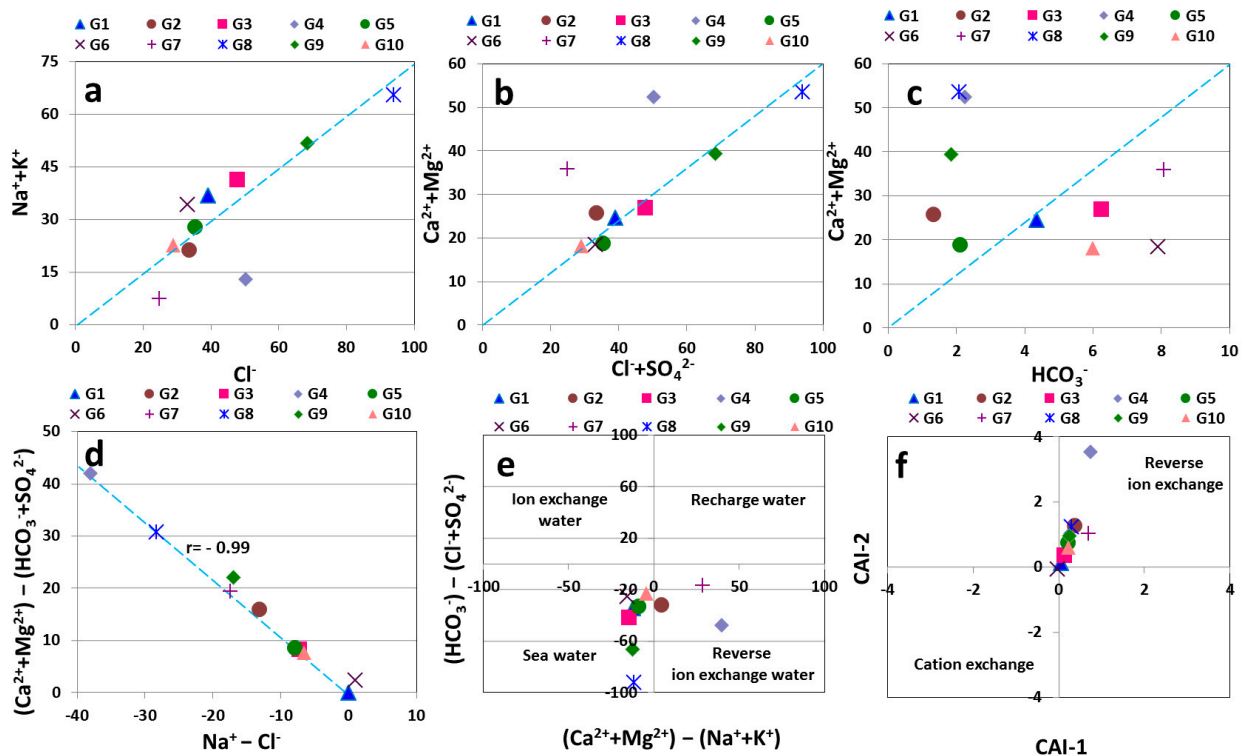


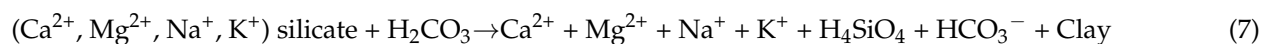
**Figure 4.** Relationships between major ions and ratios (in meq/L).

Of the alkalis,  $\text{Na}^+$  is the prevalent cation and  $\text{K}^+$  is seemingly low. In addition, there are excess alkali ions in this water (i.e., points that lie above the equiline).  $\text{K}^+$  in water naturally occurs from the weathering of igneous and sedimentary rock minerals and silicate and clay minerals [60]. The lesser presence of  $\text{K}^+$  may result from resistance of  $\text{K}^+$  to weathering and its absorption by clay minerals [61]. The  $\text{Ca}^{2+} + \text{Mg}^{2+}$  vs.  $\text{HCO}_3^- + \text{SO}_4^{2-}$  diagram shows that the majority of alkaline earth ions are balanced by bicarbonate and sulfate due to the dissolution of calcite, dolomite, and gypsum in the system. Chemical reactions as a result of ion exchange shift the points to the right of the equiline due to an excess of  $\text{HCO}_3^- + \text{SO}_4^{2-}$  [62]. If there is a greater excess of  $\text{Ca}^{2+} + \text{Mg}^{2+}$  over  $\text{HCO}_3^- + \text{SO}_4^{2-}$  ions, then points will shift to the left corner of the equiline as a result of reverse ion exchange reactions. This plot shows that a number of the points (G4 and G7 samples) lie above the 1:1 equiline, indicating excess  $\text{Ca}^{2+} + \text{Mg}^{2+}$  in these waters and that reverse ion exchange reaction has occurred in these groundwater samples.  $(\text{Ca}^{2+} + \text{Mg}^{2+}) - (\text{HCO}_3^- + \text{SO}_4^{2-})$  (Figure 4b) shows a slope of  $-0.99$  which is nearly equal to  $-1.0$ , reflecting that  $\text{Ca}^{2+}$ ,  $\text{Mg}^{2+}$ , and  $\text{Na}^+$  ions are correlative through reverse ion exchange.

The  $\text{Ca}^{2+} + \text{Mg}^{2+}$  vs.  $\text{HCO}_3^-$  diagram shows that bicarbonate is reversibly proportional to other ions in the study area (Figure 4c). The points lying above the equiline (samples G2, G4, G5, G8 and G9) are scattered, indicating that  $\text{HCO}_3^-$  is deficient in  $\text{Ca}^{2+} + \text{Mg}^{2+}$ , which needs  $\text{SO}_4^{2-} + \text{Cl}^-$  to balance the charge [63]. In addition, these samples have excess  $\text{Ca}^{2+}$  and  $\text{Mg}^{2+}$ , denoting a lower contribution of  $\text{Ca}^{2+}$  by carbonate dissolution, which can be attributed to an ion exchange reaction [42]. The  $\text{Ca}^{2+} + \text{Mg}^{2+} / \text{HCO}_3^-$  ratio (Table 3) is greater than 1 in all samples, which indicates the prevalence of alkali earth by silicate weathering over bicarbonate. The slag waste developed in producing steel (which holds large quantities of Ca, Mg, and alumina silicate) can elevate the level of  $\text{Ca}^{2+}$  and  $\text{Mg}^{2+}$  in groundwater. In addition, other anthropogenic sources such as agricultural discharge and municipal and construction waste increase Ca and  $\text{Mg}^{2+}$  ions in groundwater. Cation exchange between  $\text{Na}^+$  and  $\text{Ca}^{2+}$  could cause the plots to deviate from 1:1. The dissolved component  $\text{Ca}^{2+} / \text{Na}^+$

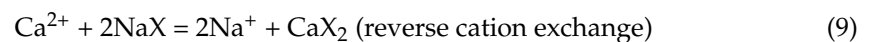
>1 (G1, G2, G3, G5, G6, G8, G9 and G10 samples) denotes  $\text{Ca}^{2+}$  extracted from silicate minerals such as plagioclases [64]. This is indicated by Figure 4d, which shows the relationship between  $(\text{Ca}^{2+} + \text{Mg}^{2+}) - (\text{HCO}_3^- + \text{SO}_4^{2-})$  as a function of  $(\text{Na}^+ - \text{Cl}^-)$ , where an excess in  $\text{Na}^+$  with respect to  $\text{Cl}^-$  and to  $\text{Ca}^{2+}$  and  $\text{Mg}^{2+}$  deficits indicates the influence of reverse ion exchange processes on modifying groundwater chemistry.

The hydro-geochemical plot proposed by Chadha [65] can assist in understanding the main geochemical processes controlling groundwater chemistry. Most samples fall within the field dominated by sea water (70%) and reverse ion exchange (30%) (Figure 4e). This can be attributed to the evaporation processes, which are the main prevalent processes that have enriched  $\text{Na}^+$  ions in regard to  $\text{Ca}^{2+}$  and  $\text{Mg}^{2+}$  ions in the investigated area. Apart from weathering process, 50% of sites were affected by precipitation and evaporation (>0.8 for  $\text{Cl}^-$  / total anion ratio). Equation (7) shows silicate weathering [32].



### 3.2.4. Ion Exchange Process

The excess  $\text{Cl}^-$  over  $\text{Na}^+$  ions in all groundwater samples (Figure 4a, Table 3) defines reverse ion exchange in an aquifer system. To identify this process in groundwater, chloro-alkaline indices were quantified (Equations (1) and (2)); the outcomes are depicted in Figure 4f. The values of CAI-1 varied from  $-0.03$  to  $0.74$ , with an average of  $0.29$ , while those of CAI-2 were from  $-0.7$  to  $3.54$ , with an average of  $0.98$ . Figure 4f shows the cation ion exchange (Equation (1)) and reverse ion exchange reactions (Equation (2)). From Figure 4, it can be observed that 90% of groundwater points toward the positive indices of CAI-1 and CAI-2. This denotes ion exchange as the main process in groundwater (Equations (8) and (9)).



### 3.2.5. Groundwater Origin

Piper's diagram (Figure 5) displays the dispersion of different cations and anions in the groundwater, denoting groundwater origin and the sources of dissolved salts while defining the lithological variations and human activities that modify the groundwater [66]. All groundwater samples fall in the upper triangle, reflecting water of secondary salinity characteristics containing  $\text{SO}_4^{2-} + \text{Cl}^- > \text{Na}^+ + \text{K}^+$ , meaning that sulfate and chloride salts prevail in this water, while bicarbonate is low. Moreover, the diagram reflects the dominance of  $\text{Ca}^{2+} + \text{Mg}^{2+}$  with  $\text{SO}_4^{2-}$  due to the dissolution of gypsum and carbonate rock minerals. The chief anion in the groundwater changes from sulfate to chloride, with a similar increase in the TDS. Two major water types can be recognized in the study area when utilizing the Piper diagram classification scheme (Figure 5).

**Ca-Mg-Cl-SO4 type:** It accounts for 30% of the samples and is a transitional type attributed to the permanent hardness class. It holds non-carbonate salts. In this facies, groundwater encounters dissolution and reverse ion exchange where  $\text{Na}^+$  in groundwater is substituted by  $\text{Ca}^{2+}$  and  $\text{Mg}^{2+}$  in the aquifer matrix. In this water type, two hydrochemical facies, i.e., Mg-Ca-Cl (G4, G7) and Na-Mg-Ca-Cl (G2), are identified.

**Na-K-Cl-SO4 type:** It accounts for 70% of the samples. It is a transitional saline water type. Halite and gypsum dissolution can provide ions to the groundwater. These salts come from the leaching of evaporites and shale through direct contact. There are five main hydrochemical facies in this type: Na-Mg-Cl-SO4 (G1), Na-Mg-Cl (G3), Na-Ca-Cl (G5, G6), Na-Mg-Ca-Cl (G8, G9), and Na-Ca-Mg-Cl (G10).

The Durov diagram [67] exhibits the groundwater composition fall in the Na-Cl waters, a distinct trend for seawater intrusion (Figure 6). This linear pattern denotes that the groundwater chemistry is affected by reverse cation exchange reactions [68]. Inspection

of the Piper and Schoeller diagrams and ion ratios shows that most alkalis ( $\text{Na}^+ + \text{K}^+$ ) run over alkaline earth ( $\text{Ca}^{2+} + \text{Mg}^{2+}$ ) and that strong acids ( $\text{SO}_4^{2-} + \text{Cl}^-$ ) surpass weak acids ( $\text{HCO}_3^- + \text{CO}_3^{2-}$ ) in the groundwater samples.

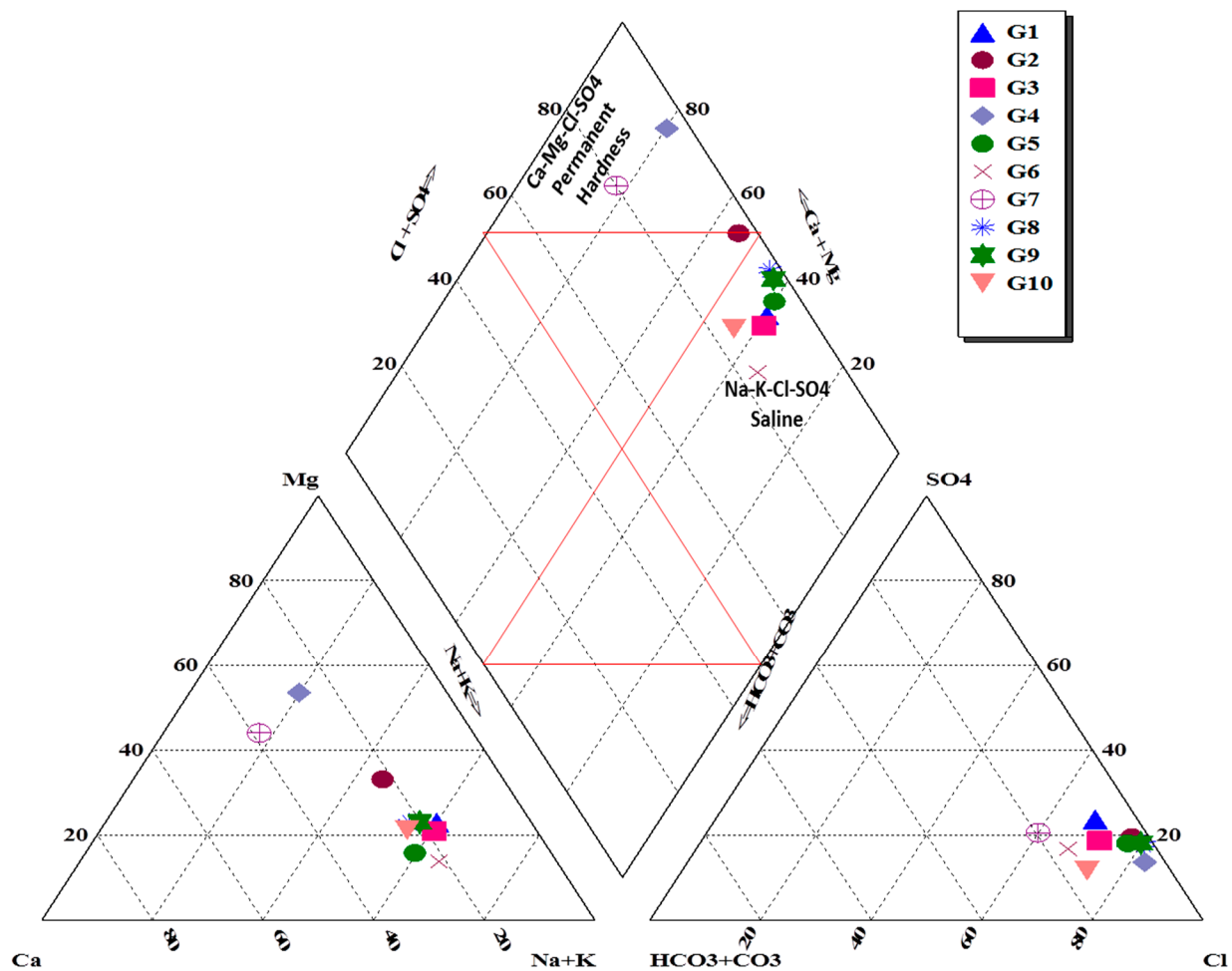


**Figure 5.** Piper trilinear diagram classifying major hydrochemical facies for groundwater samples in the investigated area.

### 3.3. Groundwater Quality

#### 3.3.1. Drinking Purpose

Groundwater appropriateness for domestic uses was quantified based on Egypt's standards [69]. The pH varies between 6.91 and 8.02 within the safe limit (6.5 to 8.5). The TDS in the investigated area is from 2450 to 6841 mg/L (Table 2), denoting that all groundwater in the investigated area surpasses the advisable limit of 1000 mg/L. Elevated TDS minimizes palatability, causes gastrointestinal irritation, and can cause kidney stones after drinking for a long period of time [70]. The  $\text{Ca}^{2+}$  quantified in the investigated area varies between 191 and 528 mg/L. Around 20% of groundwater is above the advisable limit of 350 mg/L. The values of  $\text{Mg}^{2+}$  vary between 88 and 425 mg/L; thus, about 70% of groundwater is above the advisable limit of 150 mg/L for safe water in Egypt.  $\text{Mg}^{2+}$  is an important elemental ion for enzyme activation in cells, and at elevated values is regarded as a laxative agent [70]. The values of  $\text{Na}^+$  vary from 167 to 1504 mg/L, with 90% of the samples above the advisable limit of 200 mg/L for safe water. Elevated  $\text{Na}^+$  can lead to hypertension [71].  $\text{Cl}^-$  and  $\text{SO}_4^{2-}$  are highly significant inorganic ions that can alter water quality.  $\text{Cl}^-$  plays a part in balancing the electrolyte level in the blood plasma. Elevated values can lead to hypertension, renal stones, and asthma [72]. Drinking water with elevated  $\text{SO}_4^{2-}$  values can cause diarrhea, catharsis, and

gastrointestinal irritation [70]. The groundwater in this region exhibits  $\text{Cl}^-$  and  $\text{SO}_4^{2-}$  of 877 to 3327 and 220 to 995 mg/L, respectively (Table 2), both of which surpass the standard limit for drinking water (250 mg/L).  $\text{NO}_3^-$  values were recognized in low concentrations ranging from 0.0 to 16.2 mg/L (Table 2), below the safe limit of  $\text{NO}_3^-$  in drinking water (45 mg/L).

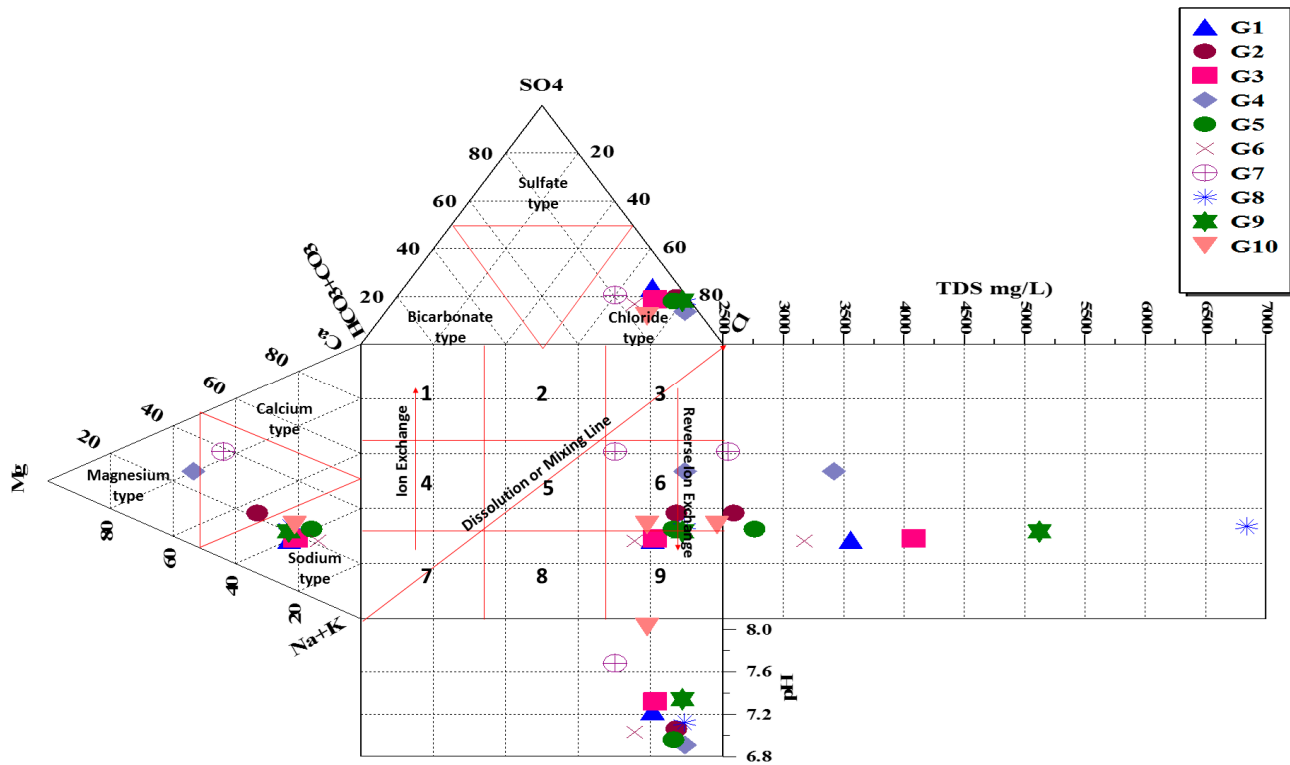


Figure 6. Durov plot depicting the hydrochemical processes involved in the investigated area Hierarchical cluster analysis (HCA) of the sampled wells.

### 3.3.2. Irrigation Purposes

The most practical parameters for managing the suitability of water for irrigation involve the total salt value and value of cations that form deflocculating clay soils with toxic impacts on plants [73].

**Salinity:** High amounts of water salts result in the development of saline soils, causing crop loss due to decreased osmotic activity of plants and consequent adsorption of water and nutrients from the soil [74]. In accordance with Ayers and Westcot [75], serious problems result recognized if water TDS is higher than 1920 mg/L. In this study, the total groundwater salinity varied from 2150 mg/L to 6841 mg/L (>1920 mg/L) (Table 2), denoting its unsuitability for irrigation based on total salinity.

**RSC:** The appropriateness of groundwater for irrigation was assessed by RSC (as a measure of  $\text{HCO}_3^-$ ), apart from the  $\text{Na}^+$  effect. As RSC rises, large amounts of  $\text{Ca}^{2+}$  and lower amounts of  $\text{Mg}^{2+}$  are precipitated out of solution when water is added to soil. The RSC values in this region vary from  $-51.57$  to  $-10.56$  meq/L (Table 3), denoting that the concentrations of  $\text{Ca}^{2+}$  and  $\text{Mg}^{2+}$  are in excess; hence, all the groundwater is safe, not hazardous, and appropriate for irrigation ( $\text{RSC} < 1.25$  meq/L).

**MH:** In the natural water system, magnesium and calcium maintain a state of equilibrium. Elevated values of magnesium and calcium can increase soil pH and decrease the infiltration capacity of soil, which affects crop yield. If the magnesium hazard content is above 50%, soil becomes alkaline and water is unsuitable for irrigation [76]. In the present study, MH values varied from 38.9 to 66.6, indicating that 70% of samples had MH values above 50. The high amount of magnesium in most samples (except G5, G6, and G10) might be due to the dissolution of carbonate rocks (Table 3).

Based on total salinity, the groundwater in the study area is unsuitable for irrigation. RSC depends on the carbonate ions only, and consequently indicates that the groundwater is suitable for irrigation. MH indicates that 70% of the wells are unsuitable. Overall, according to the salinity and MH index most wells fall into the unsuitable category of water for irrigation.

USSLS: The appropriateness of groundwater for irrigation relies on the influence of the mineral components of water on plants and soil. The  $\text{Na}^+$  value is significant in grouping irrigation water, as soils consume  $\text{Na}^+$  in exchange for  $\text{Ca}^{2+}$  and  $\text{Mg}^{2+}$ , forming clay particles that deflocculate and minimize permeability [74].

The USSLS diagram [31] assists in groundwater assessment for agricultural use, as EC acts as a salinity hazard and SAR acts as an alkalinity hazard. Applying this grouping to the groundwater in this study (Figure 7), the water samples are marked by low sodium and high salinity (C3-S1) (G6), i.e., able to be utilized for irrigation on nearly all soil types with less risk of exchangeable sodium; medium sodium and very high salinity (C4-S2) (G3, G10); high sodium and very high salinity and sodium (C4-S3) (G1, G4, G5, G9); and very high salinity (C4-S4) (G2, G7, G8), i.e., denoting a very high salinity hazard and medium to high sodium hazard, able to be used for plants only with special management such as good drainage, leaching, and incorporation of organic matter. Groundwater in C4-S2 to C4-S4 zones is of very poor quality can only irrigate plants that are highly salt-tolerant. Therefore, plants and vegetables that can tolerate high salinity, such as tomatoes, sunflower and cantaloupe, can be utilized in these areas.

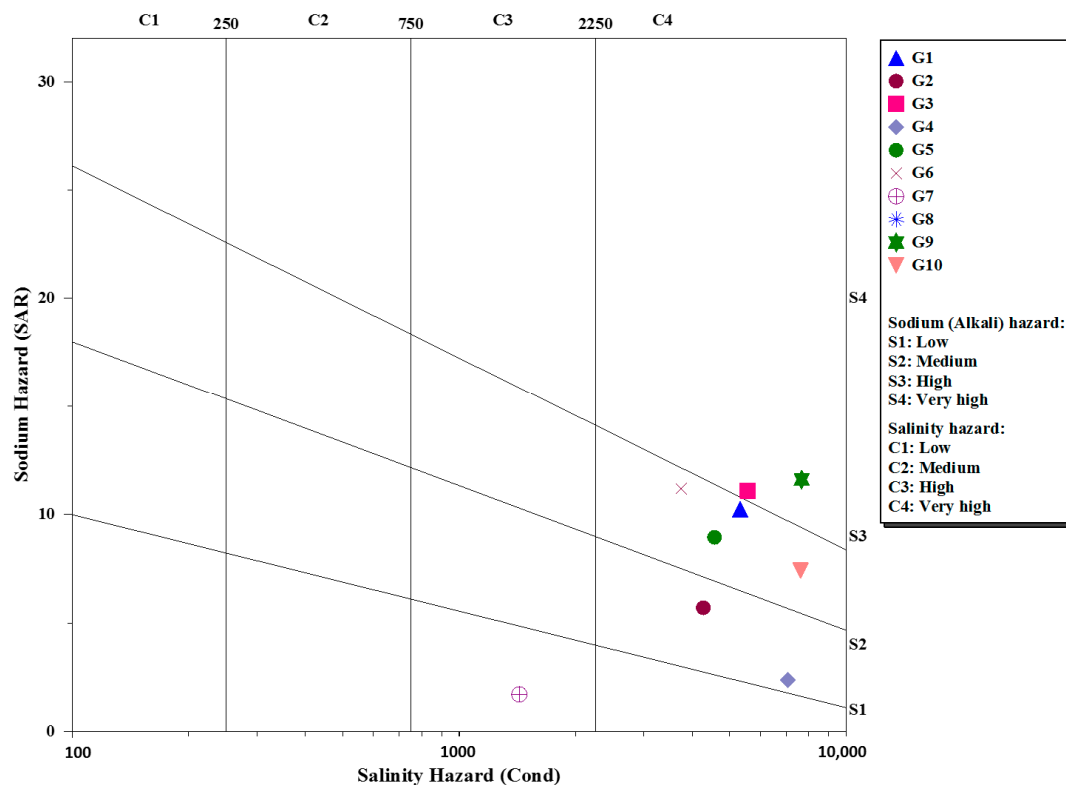


**Figure 7.** Salinity hazard classification of the sampling sites according to the US Salinity Laboratory diagram.

### 3.3.3. Industrial Purposes

The quality demands for industrial water vary greatly, and nearly every single industrial unit has specific standards. Industries are often affected by the unwanted influences of incrustation and corrosion formed by poor water quality. Incrustation includes the deposition of unwanted calcium carbonate on metal surfaces. Corrosion is a chemical activity on metals that causes deterioration of metals by chemical or electrochemical reaction. Thus,

these water quality standards have been adjusted [77] for determining the incrusting and corrosive features of water in the investigated region.

- (a) Water, with  $\text{HCO}_3^- > 400$  mg/L or TH  $> 300$  mg/L or  $\text{SO}_4^{2-} > 100$  mg/L may cause incrustation.
- (b) Water with pH  $< 7$  or TDS  $> 1000$  mg/L or  $\text{Cl}^- > 500$  mg/L may cause corrosion.

Alkalinity, pH, chloride, calcium, and sulfate are the chief water quality parameters that facilitate iron corrosion [39]. Higher concentrations of chloride and sulfate increase the rate of corrosion and pitting in iron and copper materials. Corrosion may attack a metal surface uniformly or may focused on specific sites [61]. The concentrations of both these major cations and anions were found to be high (Table 2). The  $\text{HCO}_3^-$  value surpassed the limit of 400 mg/L in about 20% of groundwater samples (G6, G7), the concentration of  $\text{SO}_4^{2-}$  was more than 220 mg/L in all groundwater samples, and the TH was higher than 900 mg/L (Table 3). Groundwater quality can cause incrustation on metal surfaces, and as such is not approved for industrial utilization. Greatly mineralized water with TDS above 1430 mg/L was found in in all groundwater samples, while  $\text{Cl}^-$  values surpassed the limit of 500 mg/L above which corrosion can develop on metal surfaces.

The CR ranged from 3.37 to 37.45 in the Quaternary aquifer and 45.06 in the Tertiary aquifer (Table 2). All sampling locations were found to have  $\text{CR} > 1$ , which denotes that water can corrode metal pipes and machinery. It is suggested that non-corrosive pipes and machinery be utilized for this water in order to protect industrial machines.

The hydrogeological conditions and chemical composition of groundwater are major constraints and limiting factors in future developments in the investigated area. The shallow groundwater systems are susceptible to pollution and have high TDS and TH, which may interfere with industrial activities. Adopting aquifer recharge procedures and rainwater harvesting in the investigated areas [78] bearing inappropriate water quality can dilute the ionic concentrations in the groundwater, which in turn will improve the quality of the groundwater for use in irrigation. More saline or salt-tolerant crops could be grown with a good irrigation system to stop soil salinization (e.g., using lime/gypsum). Regular monitoring of water quality and pollution is important for the government. This would be helpful in developing a suitable management plan and sustainable utilization of groundwater for different purposes. In addition, metal-organic frameworks (MOFs) have recently gained much attention for water treatment due to their tunable porosity, large surface area, and easily modified structure, and could be used to improve water quality in the studied areas [79,80].

#### 4. Conclusions

The present study has revealed the hydrochemical evolution, grouping, and distribution of groundwater facies in the northwestern part of the Gulf of Suez region. The average ion distribution is in the following order:  $\text{Na}^+ > \text{Mg}^{2+} > \text{Ca}^{2+} > \text{K}^+$  and  $\text{Cl}^- > \text{SO}_4^{2-} > \text{HCO}_3^-$ . The Piper trilinear diagram and Chadha's plot classified the composition of waters into two chemical types: the Ca-Mg-Cl- $\text{SO}_4$  type accounts for 30% of the samples as a result of reverse ion exchange processes, while the Na-K-Cl- $\text{SO}_4$  type accounts for 70% of the samples, reflecting the effect of evaporation. The  $\text{Ca}^{2+} + \text{Mg}^{2+} / \text{HCO}_3^-$  ratio is greater than 1 in all samples, which indicates the prevalence of alkali earth by silicate weathering over bicarbonate. The plot of  $\text{Ca}^{2+} + \text{Mg}^{2+}$  over  $\text{HCO}_3^- + \text{SO}_4^{2-}$  ions indicates an excess of  $\text{Ca}^{2+} + \text{Mg}^{2+}$  in the G4 and G7 water samples due to reverse ion exchange reactions. The values of  $r\text{Na}^+ / r\text{Cl}^-$  in the investigated zone indicate halite leaching and reverse ion exchange reactions. The heavy metal contents show enrichment of cadmium and lead that exceed the permissible values in drinking water ( $>0.003$  and  $0.01$  mg/L, respectively) due to industrial applications in the study area. For drinking purposes, the groundwater is outside of the suggested limits prescribed for drinking water. For irrigation purposes, the groundwater is safe and appropriate (RSC values  $< 1.25$  meq/L). However, based on MH values, 70% of groundwater samples were found to be unsuitable for irrigation, or suitable only for high-saline or salt-tolerant

crops. Impacts of incrustation and corrosion in groundwater at different sites are expected as well. Mineral dissolution, rock weathering, precipitation, evaporation, reverse ion exchange reactions, and anthropogenic activities are the principal factors affecting groundwater quality in the study area, requiring an appropriate management plan prior to its use.

**Author Contributions:** Conceptualization, H.A.-A., M.R. and S.R.; methodology, M.R. and S.R.; validation, H.A.-A. and M.R.; formal analysis, H.A.-A. and M.R.; investigation, M.R. and S.R.; data curation, H.A.-A. and M.R.; writing—original draft preparation, H.A.-A., M.R., and S.R.; writing—review and editing, H.A.-A., M.R. and S.R. All authors have read and agreed to the published version of the manuscript.

**Funding:** This research received no external funding.

**Institutional Review Board Statement:** Not applicable.

**Informed Consent Statement:** Not applicable.

**Data Availability Statement:** Data available on request.

**Acknowledgments:** We would like to thank the anonymous reviewers for their helpful comments, which greatly improved the manuscript.

**Conflicts of Interest:** The authors declare no conflict of interest.

## References

1. Singh, K.P.; Malik, A.; Mohan, D.; Sinha, S. Multivariate statistical techniques for the evaluation of spatial and temporal variations in water quality of Gomtiriver (India): A case study. *Water Resour.* **2004**, *38*, 3980–3992.
2. Mohamed, M.M.; Elmahdy, S.I. Natural and anthropogenic factors affecting groundwater quality in the eastern region of the United Arab Emirates. *Arabian J. Geosci.* **2015**, *8*, 7409. [[CrossRef](#)]
3. Saha, P.; Paul, B. Groundwater quality assessment in an industrial hotspot through interdisciplinary techniques. *Environ. Monit. Assess.* **2019**, *191* (Suppl. 2), 326. [[CrossRef](#)] [[PubMed](#)]
4. Alzahrani, H.; El-Sorogy, A.S.; Qaysi, S.; Alshehri, F. Contamination and Risk Assessment of Potentially Toxic Elements in Coastal Sediments of the Area between Al-Jubail and Al-Khafji, Arabian Gulf, Saudi Arabia. *Water* **2023**, *15*, 573. [[CrossRef](#)]
5. Daniele, L.; Vallejos, Á.; Corbella, M.; Molina, L.; Pulido-Bosch, A. Hydrogeochemistry and geochemical simulations to assess water–rock interactions in complex carbonate aquifers: The case of Aguadulce (SE Spain). *Appl. Geochem.* **2013**, *29*, 43–54. [[CrossRef](#)]
6. El-Moselhy, K.M.; Gabal, M.N. Trace metals in water, sediments and marine organisms from the northern part of the Gulf of Suez, Red Sea. *J. Marine Sys.* **2004**, *46*, 39–46. [[CrossRef](#)]
7. Khaled, A.; El-Nemr, A.; Said, T.O.; El-Sikaily, A.; Abd-Alla, A.M.A. Polychlorinated biphenyls and chlorinated pesticides in mussels from the Egyptian Red Sea coast. *Chemosphere* **2004**, *54*, 1407–1412. [[CrossRef](#)]
8. Nour, H.E.; Alshehri, F.; Sahour, H.; El-Sorogy, A.S.; Tawfik, M. Assessment of heavy metal contamination and health risk in the coastal sediments of Suez Bay, Gulf of Suez, Egypt. *J. Afr. Earth Sci.* **2022**, *195*, 104663. [[CrossRef](#)]
9. Snousy, M.G.; Zawrah, M.F.; Abdel-Moghny, T.H.; Ebiad, M.A.; Rashad, A.M.; Khalil, M.M.; Abu El Ella, E.M.; El-Sayed, E.; Tantawy, M.A. Mobility and Fate of Pollutants in the Aquifer System of the Northwestern Suez Gulf, Egypt. In *Reviews of Environmental Contamination and Toxicology*; De Voogt, P., Ed.; Springer: Cham, Switzerland, 2016; Volume 240. [[CrossRef](#)]
10. Hanna, R.G.M. The level of heavy metals in the Red Sea after 50 years. *Sci. Total Environ.* **1992**, *125*, 417–448. [[CrossRef](#)]
11. Abd El-Moniem, M.A.; El-Moselhy, K.M.; Hassan, S.H. Trace metals content in three fish species from Northern part of the Suez Gulf, Red Sea, Egypt. Symposium on Red Sea marine environment, Jeddah. *J. King Abdulaziz Univ. Mar. Sci.* **1994**, *7*, 15–24.
12. Hamed, M.A.; Said, T.O. Effect of pollution on the water quality of the Gulf of Suez. *Egypt. J. Aquatic Biol. Fish.* **2000**, *4*, 161–178. [[CrossRef](#)]
13. El-Sikaily, A.; Khaled, A.; El Nemr, A. Heavy metals monitoring using bivalves from Mediterranean Sea and Red Sea. *Environ. Monit. Assess.* **2004**, *98*, 41–58. [[CrossRef](#)] [[PubMed](#)]
14. Rushdi, A.I.; Kassim, T.A.T.A.; Simoneit, B.R.T. Organic tracers in sediments from the coastal zone of Ras Abu El-Darag, Gulf of Suez. *Environ. Geol.* **2009**, *58*, 1675–1687. [[CrossRef](#)]
15. Abdel-Hamid, A.M.A.; Hamed, M.A.; Abd El-Azim, H. Heavy metals distribution in the coral reef ecosystems of the Northern Red Sea. *Helgol. Mar. Res.* **2011**, *65*, 67–80.
16. Shreadah, M.A.; Said, T.O.; Abd El-Ghani, S.A.; Abd El-Moniem, M.A. Distribution of different organotin and organolead compounds in sediment of Suez Gulf. *J. Environ. Protect.* **2011**, *2*, 545–554. [[CrossRef](#)]
17. Snousy, M.G.; Zawrah, M.F.; Rashad, A.M.; Ebiad, M.A.; El-Sayed, E.; Tantawy, M.A. HPLC evaluation of PAHS polluted soil in coastal petroleum refinery site Northwestern Suez Gulf, Egypt. *Res. J. Environ. Toxicol.* **2015**, *9*, 251–260.

18. Conoco Geologic Map of Egypt. Egyptian General Authority for Petroleum (UNESCO Joint Map Project), 20 Sheets, Scale 1500, 000, Cairo, 1987. Available online: <https://shop.geospatial.com/product/N1QHZXNQC4BQ4FTWS6H8FPCXJ4/03-EGAC-N1QH-Egypt-1-to-500000-Scale-Geological-Maps> (accessed on 13 July 2023).
19. El-Behiry, M.G.; Shedid, A.; Abu-Khadra, A.; El-Huseiny, M. Integrated GIS and remote sensing for runoff hazard analysis in Ain Sukhna industrial area, Egypt. *JKAU Earth Sci.* **2006**, *17*, 19–42. [[CrossRef](#)]
20. Abdallah, A.M.; Abd El-Hady, F.M. Geology of Sadat area, Gulf of Suez. *UAR J. Geol.* **1966**, *10*, 1–24.
21. Mohamed, A.M.E. Estimating Earthquake Ground Motions at the Northwestern Part of the Gulf of Suez, Egypt. Ph.D. Thesis, Ain Shams University, Cairo, Egypt, 2003.
22. Sultan, M.; Metwally, S.; Milewski, A.; Becker, D.; Ahmed, M.; Sauck, W.; Soliman, F.; Sturchio, N.; Yan, E.; Rashed, M.; et al. Modern recharge to fossil aquifers: Geochemical, geophysical, and modeling constraints. *J. Hydrol.* **2011**, *403*, 14–24. [[CrossRef](#)]
23. EMA (Egyptian General Authority of Meteorology). Available online: <http://ema.gov.eg/> (accessed on 4 July 2023).
24. American Public Health association (APHA). *Standard Methods for the Examination of Water and Wastewater*, 22nd ed.; American Water Works Association: Washington, DC, USA, 2012; 1496p.
25. REGWA. *Groundwater Resources in Wadi Badaa and Wadi Hagul*; Internal Report; REGWA: Cairo, Egypt, 1979.
26. Schoeller, H. Geochemistry of Groundwater. In *Groundwater Studies—An International Guide for Research and Practice*; UNESCO: Paris, France, 1977.
27. Deepali, M.; Malpe, D.B.; Subba Rao, N. Identification of controlling processes of groundwater quality in a developing urban area using principal component analysis. *Environ. Earth Sci.* **2015**, *74*, 5919–5933. [[CrossRef](#)]
28. Singh, A.K.; Mondal, G.C.; Kumar, S.; Singh, T.B.; Tewary, B.K.; Sinha, A. Major ion chemistry, weathering processes and water quality assessment in upper catchment of Damodar River basin, India. *Environ. Geol.* **2008**, *54*, 745–758. [[CrossRef](#)]
29. Eaton, E.M. Significance of carbonates in irrigation waters. *Soil Sci.* **1950**, *69*, 123–133. [[CrossRef](#)]
30. Szabolcs, I.; Darab, C. The influence of irrigation water of high sodium carbonate content of soils. In Proceedings of the 8th International Congress of ISSS, Tsukuba, Japan, 9 September 1964; pp. 803–812.
31. US Salinity Laboratory Staff (USSLS). *Diagnosis and Improvements of Saline and Alkali Soils*; US Department of Agriculture Handbook; USDA: Washington, DC, USA, 1954; No. 60, p. 160.
32. Patel, P.; Raju, N.J.; Reddy, B.C.S.R.; Suresh, U.; Gossel, W.; Wycisk, P. Geochemical processes and multivariate statistical analysis for the assessment of groundwater quality in the Swarnamukhi River basin, Andhra Pradesh, India. *Environ. Earth Sci.* **2016**, *75*, 1–24. [[CrossRef](#)]
33. Desouki, H.A.; Gomaa, M.A.; Sadek, M.A.; Ezz El-Deen, H.A. Hydrochemical and isotopic evaluation of groundwater quality, El Ain El—Sukhna and Wadi Araba localities, aquifers, Egypt. *Mansoura J. Geol. Geophys.* **2006**, *33*, 32–64.
34. Abdel Raouf, A.U. Geophysical Studies on Wadi Hagul-Wadi Badaa Area, North of Ain Sukhna, Gulf of Suez. Ph.D. Thesis, Faculty of Science, Mansoura University, Mansourah, Egypt, 2001; 199p.
35. Elewa, H.H. A strategy for optimizing groundwater recharging by flood water in the northwestern coastal zone of the Gulf of Suez, Egypt. In Proceedings of the 5th International Symposium on Management of Aquifer Recharge (ISMAR 5), Berlin, Germany, 10–16 June 2005.
36. Tóth, J. Groundwater as a geologic agent: An overview of the causes, processes, and manifestations. *Hydrogeol. J.* **1999**, *7*, 1–14. [[CrossRef](#)]
37. Singh, S.; Raju, N.J.; Ramakrishna, C. Evaluation of groundwater quality and its suitability for domestic and irrigation use in parts of the Chandauli-Varanasi region, Uttar Pradesh, India. *J. Water Resour. Protect.* **2015**, *7*, 572–587. [[CrossRef](#)]
38. Batayneh, A.T.; Al-Taani, A.A. Integrated resistivity and water chemistry for evaluation of groundwater quality of the Gulf of Aqaba coastal area in Saudi Arabia. *J. Geosci.* **2016**, *20*, 403–413. [[CrossRef](#)]
39. World Health Organization (WHO). *Guidelines for Drinking-Water Quality*, 4th ed.; World Health Organization: Geneva, Switzerland, 2011; 564p, ISBN 9789241548151.
40. Ahmed, A.A.; Ali, M.H. Hydrochemical evolution and variation of groundwater and its environmental impact at Sohag, Egypt. *Arab. J. Geosci.* **2011**, *4*, 339–352. [[CrossRef](#)]
41. Edet, A.E.; Worden, R.H.; Mohammed, E.A.; Preston, M.R. Hydrogeochemical processes in a populated shallow coastal Plain Sand Aquifer, Southeastern Nigeria. *Environ. Earth Sci.* **2012**, *65*, 1933–1953. [[CrossRef](#)]
42. Elgano, L.; Kannan, R. Rock–water interaction and its control on chemical composition of groundwater. In *Developments in Environmental Science*; Sarkar, D., Datta, R., Hannigan, R., Eds.; Elsevier: Amsterdam, The Netherlands, 2007; Chapter 11; Volume 5, pp. 229–243.
43. Fallatah, O.; Khatlab, M.R. Evaluation of Groundwater Quality and Suitability for Irrigation Purposes and Human Consumption in Saudi Arabia. *Water* **2023**, *15*, 2352. [[CrossRef](#)]
44. Cushing, E.M.; Kantrowitz, I.H.; Taylor, K.R. *Water Resources of the Delmarva Peninsula*; U.S. Geological Survey: Reston, VA, USA, 1973; Professional Paper 822; 58p.
45. Qian, J.Z.; Wang, L.L.; Zhan, H.B.; Chen, Z. Urban land-use effects on groundwater phosphate distribution in a shallow aquifer, Nanfei River basin, China. *Hydrogeol. J.* **2011**, *19*, 1431–1442. [[CrossRef](#)]
46. Eickhout, B.; van Meijl, H.; Tabeau, A.; Van Rheenen, T. Economic and ecological consequences of four European land-use scenarios. *Land Use Policy J.* **2007**, *24*, 562–575. [[CrossRef](#)]

47. Wei, Y.; Fan, W.; Wang, W.; Deng, L. Identification of nitrate pollution sources of groundwater and analysis of potential pollution paths in loess regions: A case study in Tongchuan region, China. *Environ. Earth Sci.* **2017**, *76*, 423. [[CrossRef](#)]
48. Jalali, M. Geochemistry characterisation of groundwater in an agricultural area of Razan, Hamadan, Iran. *Environ. Geol.* **2009**, *56*, 1479–1488. [[CrossRef](#)]
49. Kilemtov, P.P. *General Hydrology*; Mir Publishers: Moscow, Russia, 1983; 239p.
50. Mapoma, H.W.T.; Xie, X.; Nyirenda, M.T.; Zhang, L.; Kaonga, C.C.; Mbewe, R. Trace elements geochemistry of fractured basement aquifer in southern Malawi: A case of Blantyre rural. *Afric. Earth Sci.* **2017**, *131*, 43–52. [[CrossRef](#)]
51. Mielke, H.W.; Adams, J.L.; Chaney, R.L.; Mielke, P.W.; Ravlukumar, V.C. The pattern of cadmium in the environment of five Minnesota cities. *Environ. Geochem. Health* **1991**, *13*, 29–34. [[CrossRef](#)]
52. Liao, F.; Wang, G.; Shi, Z.; Huang, X.; Xu, F.; Xu, Q.; Guo, L. Distributions, sources, and species of heavy metals/trace elements in shallow groundwater around the Poyang Lake, East China. *Expo Health* **2018**, *10*, 211. [[CrossRef](#)]
53. Tebutt, T.H.Y. *Relationship between Natural Water Quality and Health*; UNESCO: Paris, France, 1983.
54. Schoeller, H. Qualitative evaluation of groundwater resources. In *Methods and Techniques of Groundwater Investigation and Development*; UNESCO: Delft, The Neatherland, 1965; Series-33; pp. 54–83.
55. Belkhir, L.; Mouni, L. Hydrochemical analysis and evaluation of groundwater quality in El Eulma area, Algeria. *Appl. Water Sci.* **2012**, *2*, 127–133. [[CrossRef](#)]
56. Lawrence, A.R.; Lloyd, J.W.; Marsh, J.M. Hydrochemistry and ground-water mixing in part of the Lincolnshire limestone aquifer. *Engl. Groundw.* **1967**, *14*, 1023–1045. [[CrossRef](#)]
57. Djorfi, S.; Djorfi, S.; Beloulou, L.; Djidel, M.; Guechi, S. Hydrochemical Evolution of Groundwater in the Tamlouka Plain, Influence of Lithology, Geomorphology and Anthropogenic Actions. In *Recent Advances in Environmental Science from the Euro-Mediterranean and Surrounding Regions*; Kallel, A., Ksibi, M., Ben Dhia, H., Khélifi, N., Eds.; EMCEI 2017. Advances in Science, Technology & Innovation (IEREK Interdisciplinary Series for Sustainable Development); Springer: Cham, Switzerland, 2018.
58. Meybeck, M. Global chemical weathering of surficial rocks estimated from river dissolved loads. *Am. J. Sci.* **1987**, *287*, 401–428. [[CrossRef](#)]
59. Atta, S.A.; Sharaky, A.M.; ElHassanein, A.S.; Khallaf, K.M.A. Salinization of the groundwater in the coastal shallow aquifer, Northwestern Nile Delta, Egypt. In Proceedings of the 1st International Conference on the Geology of Tethys, Cairo University, Cairo, Egypt, 11–14 November 2005; pp. 151–166.
60. Howari, F.M.; Banat, K.M. Hydrochemical characteristics of Jordan and Yarmouk River waters: Effect of natural and human activities. *J. Hydrol. Hydromech.* **2002**, *50*, 50.
61. Sarin, M.M.; Krishnaswamy, S.; Dilli, K.; Somayajulu, B.L.K.; Moore, W.S. Major-ion chemistry of the Ganga-Brahmaputra river system: Weathering processes and fluxes to the Bay of Bengal. *Geochim. Cosmochim. Acta* **1989**, *53*, 997–1009. [[CrossRef](#)]
62. Fisher, S.R.; Mulligan, W.F. Hydrogeochemical evaluation of sodium-sulphate and sodium-chloride groundwater beneath the northern Chihuahua desert, Trans-Pecos, Texas, USA. *Hydrogeol. J.* **1997**, *5*, 4–16. [[CrossRef](#)]
63. Das, B.K.; Kaur, P. Major ion chemistry of Renuka Lake and weathering processes, Sirmaur district, Himachal Pradesh, India. *Environ. Geol.* **2001**, *40*, 908–917. [[CrossRef](#)]
64. Li, P.; Wu, J.; Qian, H. Hydrogeochemistry and quality assessment of shallow groundwater in the southern part of the Yellow River Alluvial Plain (Zhongwei Section), China. *Earth Sci. Res. J.* **2014**, *18*, 27–38. [[CrossRef](#)]
65. Chadha, D.K. A proposed new diagram for geochemical classification of natural waters and interpretation of chemical data. *Hydrogeol. J.* **1999**, *7*, 431–439. [[CrossRef](#)]
66. Piper, A.M. A graphical procedure in the geochemical interpretation of water analysis. *Transact. Am. Geophys. Union* **1944**, *25*, 914–923. [[CrossRef](#)]
67. Zaporozec, A. Graphical interpretation of water-quality data. *Ground Water* **1972**, *10*, 32–43. [[CrossRef](#)]
68. Murad, A.A.; Garamoon, H.; Hussein, S.; Al-Nuaimi, H.S. Hydrogeochemical characterization and isotope investigations of a carbonate aquifer of the northern part of the United Arab Emirates. *J. Asian Earth Sci.* **2011**, *40*, 213–225. [[CrossRef](#)]
69. Ministry of Water Resources and Irrigation (MWRI). *Guidelines Regarding Protection of the Nile River and Water Resources from the Pollution, Egypt, Law 48/1982*; Ministry of Water Resources and Irrigation: Cairo, Egypt, 2009; Decision No. 402.
70. Garg, V.K.; Suthar, S.; Singh, S.; Sheoran, A.; Garima, M.; Jai, S. Drinking water quality in villages of southwestern Haryana, India: Assessing human health risks associated with hydrochemistry. *Environ. Geol.* **2009**, *58*, 1329–1340. [[CrossRef](#)]
71. He, F.J.; MacGregor, G.A. A comprehensive review on salt and health and current experience of worldwide salt reduction programmes. *J. Human Hypertens.* **2009**, *23*, 363–384. [[CrossRef](#)] [[PubMed](#)]
72. McCarthy, M.F. Should we restrict chloride rather than sodium? *Med. Hypothesis* **2004**, *63*, 138–148. [[CrossRef](#)] [[PubMed](#)]
73. Subba Rao, N.; Surya Rao, P.; Venktram Reddy, G.; Nagamani, M.; Vidyasagar, G.; Satyanarayana, N.L. Chemical characteristics of groundwater and assessment of groundwater quality in Varaha River Basin, Visakhapatnam District, Andhra Pradesh, India. *Environ. Monit. Assess.* **2012**, *184*, 5189–5214.
74. Shrivastava, P.; Kumar, R. Soil salinity: A serious environmental issue and plant growth promoting bacteria as one of the tools for its alleviation. *Saudi J. Biol. Sci.* **2015**, *22*, 123–131. [[CrossRef](#)]
75. Ayers, R.S.; Westcot, D.W. *Water Quality for Agriculture*; FAO Irrigation and Drainage Paper 29; FAO: Rome, Italy, 1976; 97p.
76. Nagaraju, A.; Sunil Kumar, K.; Thejaswi, A. Assessment of groundwater quality for irrigation: A case study from Bandalamottu lead mining area, Guntur district, Andhra Pradesh, South India. *Appl. Water Sci.* **2014**, *4*, 385–396. [[CrossRef](#)]

77. Johnson, E.E. *Groundwater and Wells*, 1st Indian ed.; Jain Brothers: Udaipur, India, 1983; 440p.
78. Mukherjee, I.; Singh, U.K.; Chakma, S. Evaluation of groundwater quality for irrigation water supply using multi-criteria decision-making techniques and GIS in an agroeconomic tract of Lower Ganga basin, India. *J. Environ. Manag.* **2022**, *309*, 114691. [[CrossRef](#)]
79. Khan, M.S.; Shahid, M. Improving Water Quality Using Metal–Organic Frameworks. In *Metal–Organic Frameworks for Environmental Remediation*; American Chemical Society: Washington, DC, USA, 2021; pp. 171–191. [[CrossRef](#)]
80. Shi, Y.; Zou, Y.; Khan, M.S.; Zhang, M.; Yan, J.; Zheng, X.; Wang, W.; Xie, Z. Metal–organic framework-derived photoelectrochemical sensors: Structural design and biosensing technology. *J. Mater. Chem. C* **2023**, *11*, 3692–3709. [[CrossRef](#)]

**Disclaimer/Publisher’s Note:** The statements, opinions and data contained in all publications are solely those of the individual author(s) and contributor(s) and not of MDPI and/or the editor(s). MDPI and/or the editor(s) disclaim responsibility for any injury to people or property resulting from any ideas, methods, instructions or products referred to in the content.